GMI
GeoMechanics International

Wellbore Stability and Natural Fracture Permeability in the Alum Geothermal Project, Well 25-29, Nevada

Memo submitted to
Sierra Geothermal Power Corporation (SGP)
March 2010

Confidential

Prepared by: Daniel Moos & Laura Hynes

Disclaimer

Neither GeoMechanics International, Inc. nor any person acting on behalf of GeoMechanics International:

1. Makes any warranty or representation, express or implied, with respect to the accuracy, completeness, or usefulness of the information contained in this report, or that the use of any apparatus, method, or process disclosed in this report may not infringe privately owned rights; or
2. Assumes any liability with respect to the use of, or for damages resulting from the use of, any information, apparatus, method, or process disclosed in this report.

Introduction

GeoMechanics International, Inc. (GMI) was contracted by Sierra Geothermal Power Corporation to build a geomechanical model to evaluate natural fracture and fault permeability at the Alum Geothermal Project Site, Nevada. A comprehensive suite of downhole data was acquired in the Alum 25-29 well, including leakoff tests, standard logs (density, neutron, GR, resistivity), repeated temperature logs, a cross dipole acoustic log, and digital STAR™ and CBIL™ wellbore image data. This data was analyzed by GMI to detect wellbore failures (breakouts and drilling-induced tensile wall fractures), acoustic anisotropy, and the locations and characteristics of natural fractures. Using the results of this analysis a geomechanical model was built and then used to evaluate natural fracture and fault permeability using the "critically stressed fracture" concept. Figure 1 shows the location of the Alum site and the orientation of the maximum horizontal stress determined in this study.

The Alum 25-29 well was drilled from a surface location that is NW and down-dip from the surface trace of the Alum detachment fault which separates volcaniclastic and other sediments above from crystalline rocks below. The well penetrated nearly 600 meters of sediments, crossed a shallowly NW-dipping fault zone, and entered basement. After casing was set at 691 meters MD, drilling continued to a total depth of 1,000 meters MD. In order to increase the likelihood of intersecting vertical natural fractures, and to better constrain the in situ stress state, the well was kicked off to the South at approximately 800 m, reaching a maximum deviation of 15 degrees at 930 m and holding angle to total depth.

A Note About this Memo

This memo provides a brief description of the data and methods used in the study, followed by key findings, implications, recommendations, and a few key figures. Note that numerous additional figures that are not described in this document can be found in the accompanying PowerPoint presentation. References to diagrams contained in the Memo are referred to as 'Figures', and references to diagrams contained in the PowerPoint are referred to as 'Slides'.

Data

A summary of the data collected in the Alum 25-29 well can be found in Slide 11 of the accompanying presentation. The available data included: standard log data (see Slide 21), STAR™/CBIL™ image data (examples of which are shown in Slides 24-30), and XMAC™ acoustic and crossed dipole data (presented for comparison with other analyses in Slides 36 & 37), reports, maps and cross-sections of the site (Slides 7-10), cuttings analyses (which were used to prepare the lithology logs shown in Slides 13, 21 and 22), daily drilling reports (see Slide 13), pressure records of an FIT at 157 m MD and an extended LOT (leakoff test) at 691 m MD (for a discussion of these tests see Slides 14-19). Temperature logs were recorded repeatedly to monitor recovery of the drilling-perturbed in situ profile. These are shown along

with the other logs in Track 4 of Slide 21. Figure 2 shows the log data along with a stratigraphic column.

Methods

The data summarized above from the Alum 25-29 well was reviewed, quality controlled, and collated prior to analysis. Figure 3 shows examples of the image data acquired in the sediments and basement. Examples of bedding and fracturing can be seen in Slides 24 and 25, which also highlight the differences and compare the benefits of acoustic and electrical image data. Images of the detachment fault are shown in Slide 26. The CBIL and STAR image data were then analyzed to detect and orient bedding, fractures and faults. The results are summarized for the upper and lower logging runs on Slides 31 and 33, respectively. Poles to fractures and bedding are shown in lower hemisphere stereographic projections in Figure 4.

Drilling-induced wellbore breakouts and tensile fractures were identified at a number of depths (see Slides 27-29) and provided excellent constraints on the orientations of the least (S_{hmin}) and greatest (S_{Hmax}) horizontal principal stresses, as well as providing confirmation that the stresses are not rotated away from the vertical in spite of the fact that the bedding dips to the southeast and the detachment fault dips to the northwest.

Figure 4 shows the orientations of the maximum horizontal stress determined separately for the upper and lower sections and from breakouts and induced tensile wall fractures. The stress orientations derived from these features are consistent in all cases, and indicate that S_{Hmax} is oriented NE-SW, approximately in the strike direction of bedding and of the fault. This is the predominant fast direction detected in cross dipole acoustic logs. This is also the strike direction of bedding and of the predominant set of conjugate basement fractures (Slides 36-41). While it is possible that anisotropy in the sediments is stress-induced, anisotropy in basement can only be due to the orientations of steeply dipping, compliant natural or induced fractures.

Using logging data, we determined the vertical stress and the mechanical rock properties. The vertical stress magnitude is derived by integrating the density logs. Mechanical rock properties are derived from sonic velocities using empirical relationships and are important for computing the stress magnitudes from the characteristics of wellbore failures. The elastic properties and strength computed from the logging data (strength is computed from acoustic velocity using relationships that have been validated in numerous other studies) are shown in Slide 22. Analysis of the extended LOT at 691 meters provided a measure of the magnitude of the least principal stress, S_{hmin} (see Slides 16-18). Features that might be traces of the hydraulic fractures induced during this test are visible in the image log shown in Slide 19.The pore pressure in this region is sub-hydrostatic; the reported water table is approximately 187 meters (600 feet) below the surface. This has been confirmed by monitoring the height of water in the wellbore during acquisition of temperature logs as it slowly recovered to equilibrium during the months after the well was completed.

Once the vertical stress, the least principal horizontal stress, the pore pressure, and the stress orientation are constrained, the magnitude of S_{Hmax}, which cannot be directly measured, is

computed from the characteristics of wellbore failures (see Slide 43) using the log-derived strength properties . Examples of the computation of S_{Hmax} magnitude determined by modeling the failure observed in the image data using the stress modeling software GMI-SFIB™ are shown in slides 44 through 47. The stress state consistent with all of the available information is normal faulting ($S_{hmin}<S_{Hmax}<S_v$), as indicated by the pink squares that span the range of possible stresses in Slides 44, 46, and 47. Figure 5 shows a CSTR analysis.

Using the results of the above analyses of stress and fractures, the likelihood that fractures and faults are hydraulically conductive can be determined. The analysis is based on the fact that faults and fractures with high resolved shear-to-normal stress ratios, which are likely to be active in the current stress field (i.e., are critically stressed) are more likely to be hydraulically conductive than fractures and faults which are not critically stressed. This is because repeated small slip events that occur on critically stressed fractures re-open fractures that over geological time will be sealed by alteration products. This process is most active in upwelling geothermal zones. Results of previously published studies of geothermal fields in western Nevada confirm this model.

GMI utilizes GMI•MohrFracs™ to combine the results of our detailed stress analysis with the orientations of natural fractures determined from wellbore image data to compute the normal and shear tractions acting on each fracture plane. Summary results of this analysis are shown in Slides 50 and 51. Figure 6 shows an example of a MohrFracs analysis.

Key Findings

Geomechanical Model

- The orientation of S_{Hmax} is N295°E, and the tectonic stress regime is normal faulting: ($S_v>S_{Hmax}>S_{hmin}$).
- S_{hmin} is no less than 11.5 ppg equivalent, This is too large to trigger active seismicity except on very weak, well-oriented, cohesionless faults.
- S_{Hmax} magnitude is approximately 16 to 17 ppg equivalent.
- Pore pressure is sub-hydrostatic.

Bedding, Faults, and Fractures

- The detachment fault zone which separates basement from overlying sediments is characterized by the presence of a “soft” band at 592.5 m which dips 26° towards N295°E. Based on temperature profiles, upwards cross flow is concentrated below this band.

- Bedding above the fault dips approximately 40 degrees towards the SE.

- Fractures are concentrated within the uppermost 300 meters of basement, and rare in the overlying sediments rock and at greater depths below the fault. In the sediments fractures are generally antithetic to the structural dip, whereas both SE and NW dipping fractures occur in basement. Higher GR intervals in basement are in general more heavily fractured than those with lower GR. Fractures in basement below the uppermost zone, many of which may be picked along mylonitic bands, are mechanically and hydrologically unimportant.

- Many of the fracture planes are optimally oriented for slip but aren't active unless very weak.

- The fault is poorly oriented for slip.

Wellbore stability, stress-induced failure, and anisotropy

- No instabilities were encountered while drilling the Alum 25-29 well using a mud density close to that of pure water; however, several episodes of lost circulation occurred over the interval 660-700 m MD.

- A few scattered breakouts occurred in shallow sediments, and there was one breakout interval in upper basement.

- Induced tensile fractures occur intermittently in the uppermost basement.

- The orientations of breakouts and tensile features are consistent with each other

- Dipole mode anisotropy in the sediments is aligned with the strike direction of bedding. This is also 90° to the orientation of wellbore breakouts. This orientation could be controlled either by structure or stress.

- In basement, anisotropy is not stress-induced but is weakly correlated and aligned with vertical tensile fractures and steeply dipping natural fractures

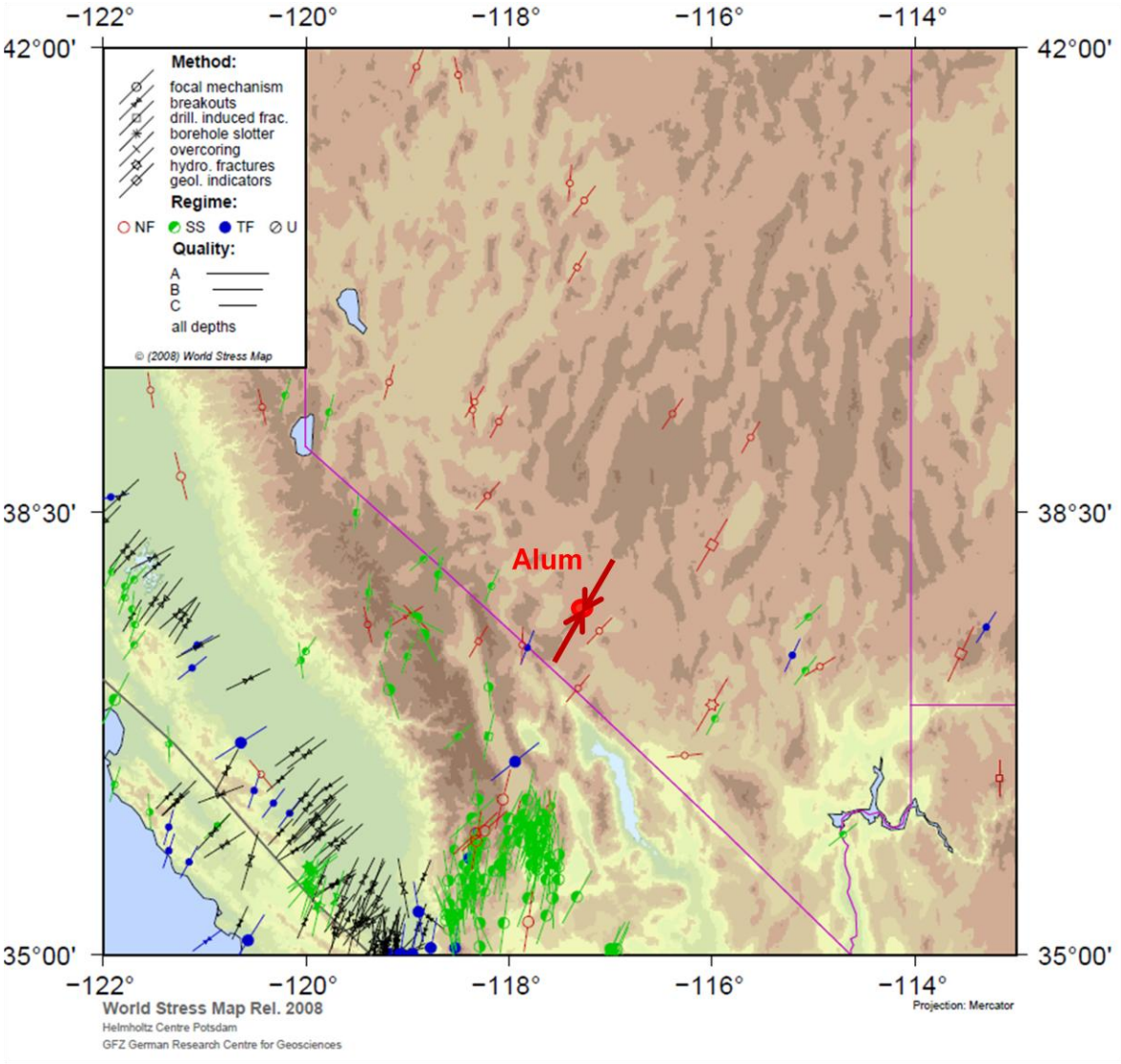

Figure 1: Location of the Alum site and the orientation of S_{Hmax} determined in this study. This orientation is consistent with other nearby stress indicators.

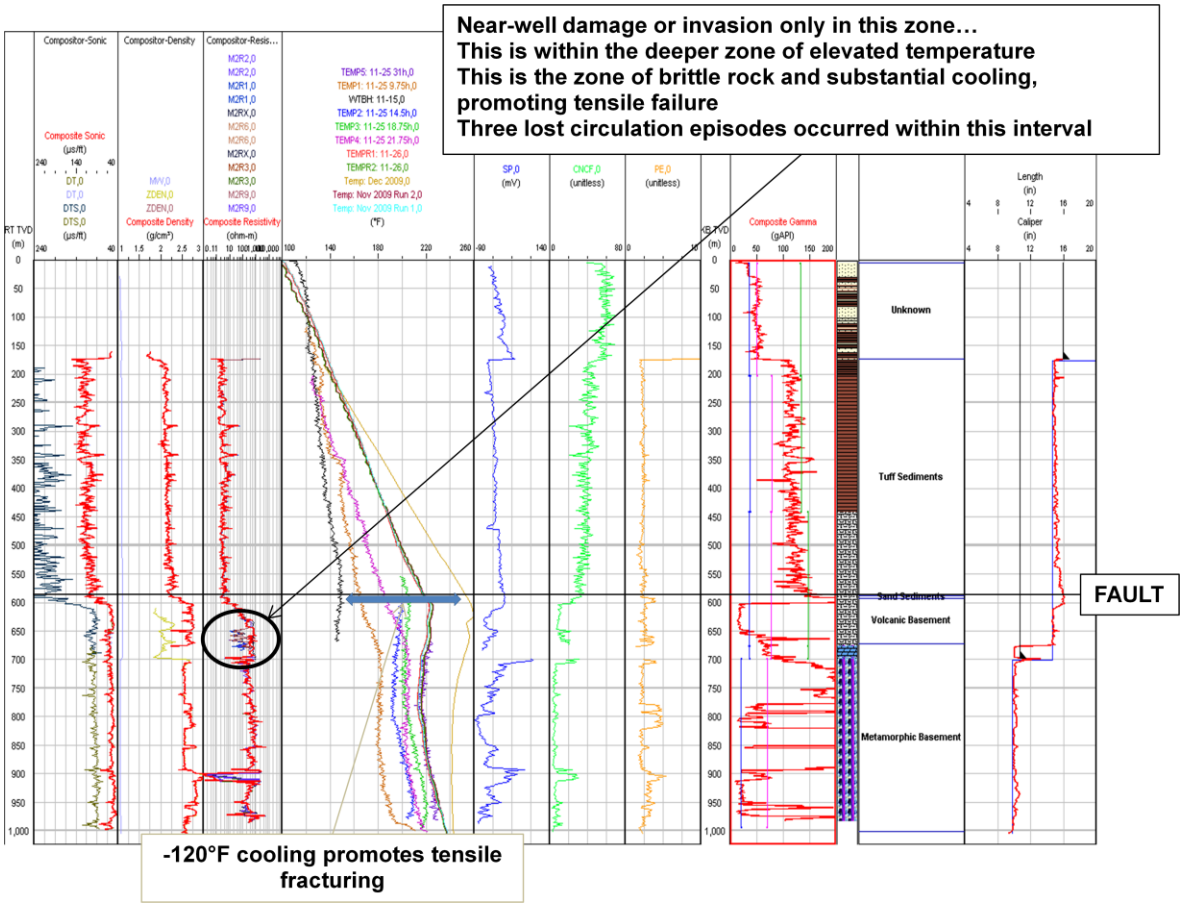

Figure 2. Summary plot of logs and stratigraphy in Alum 25-29.

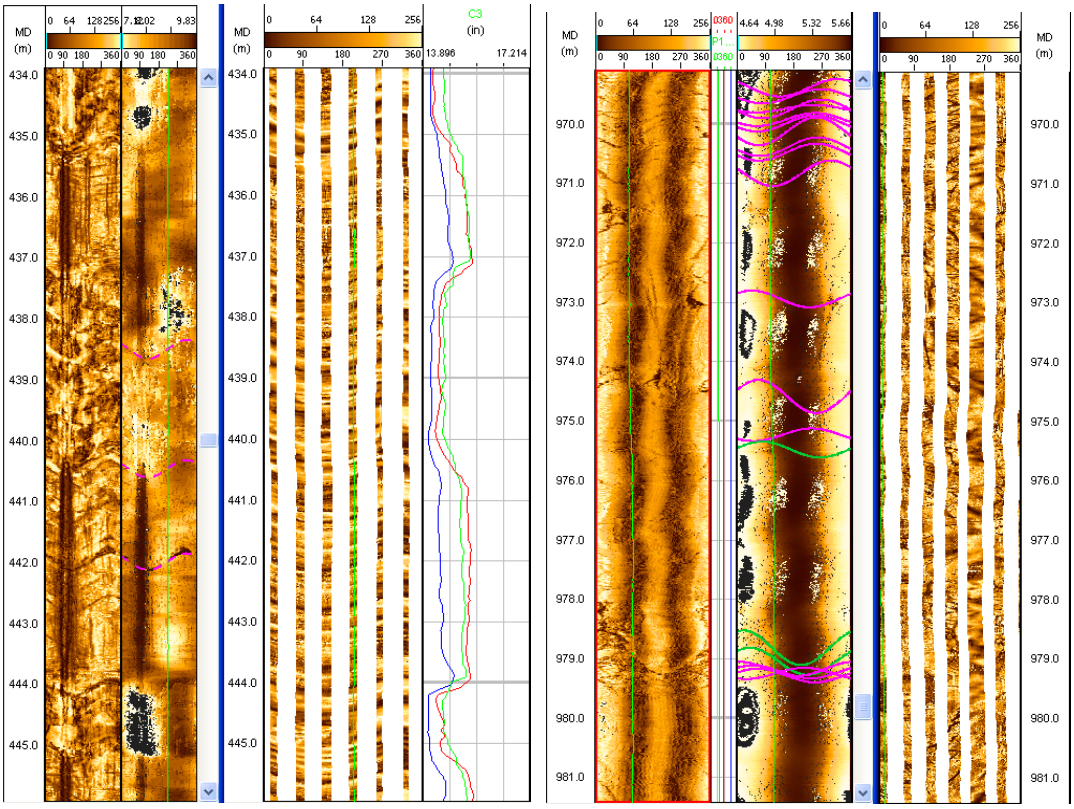

Figure 3: Wellbore image examples comparing the CBIL and STAR tools in sediments (left, along with caliper data) and basement (right). The CBIL acoustic data does detect bedding boundaries, and also detects differences between the characteristics of intervals within which the wellbore diameter is larger vs. those in which it is smaller. However, the STAR electrical image provides much better delineation of fine-scale stratigraphy. Fractures in basement are visible on the CBIL data, but are difficult to separate on the electrical (STAR) images from the highly complex fabric.

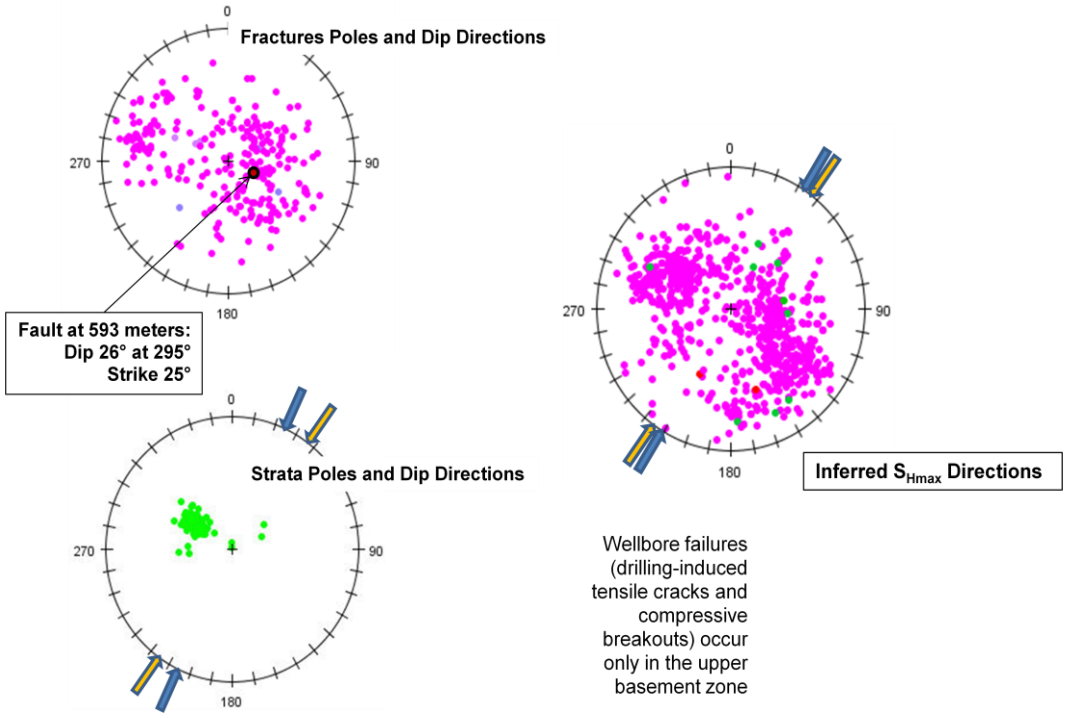

Figure 4: Fracture (magenta), bedding (green), and stress orientation (arrows) in the logged section above the final casing shoe (left) and in the deeper logged section (right). Fractures and bedding orientations are poles to the feature planes plotted on a lower-hemisphere stereographic projection. Strata (lower left) dip shallowly towards the southwest. Relatively few fractures were detected in sediments – most of the fractures in the upper left image occur below the fault, in the lowermost 150 meters of the logged section. Most of the fractures in the upper-right figure occur within the uppermost 150 meters of the logged section (i.e., within 300 meters of the fault). Fractures in basement have strong preferred NE-SW strikes, and form a conjugate pair of NW and SE dipping planes. The arrows indicate the orientation of S_{Hmax} determined from breakouts (blue) and drilling-induced tensile wall fractures (orange). This is the strike direction of bedding, of the fault, and of the majority of basement fractures.

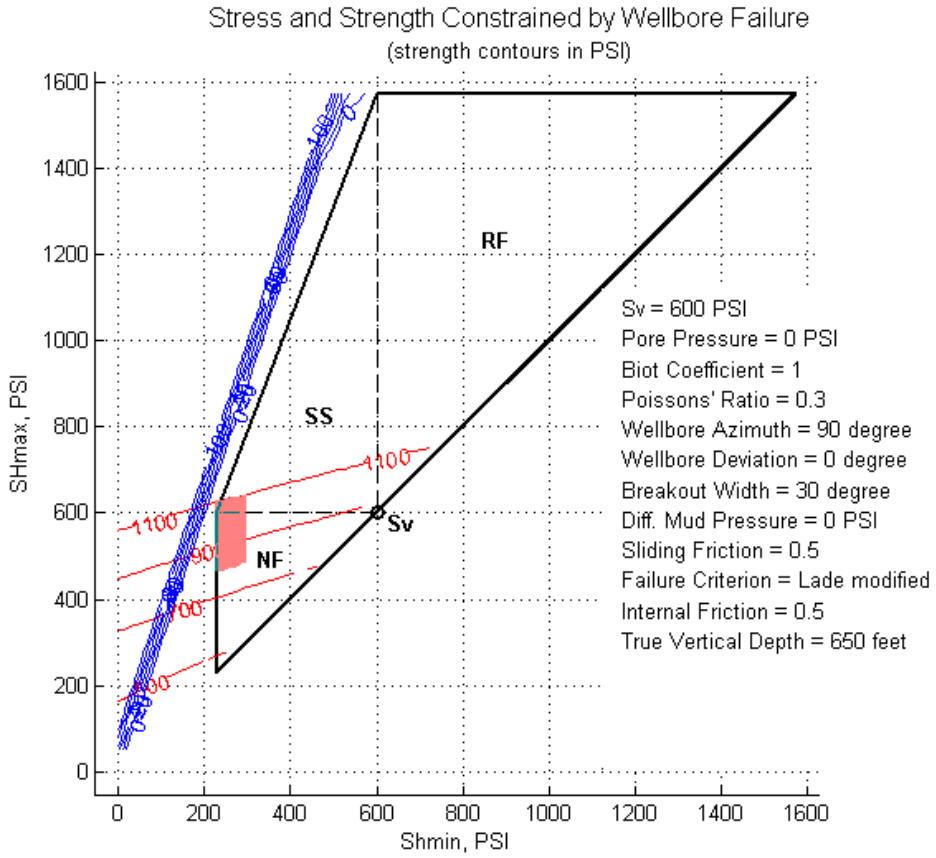

Figure 5: Example of a CSTR analysis carried out using GMI•SFIB™, showing in pink the range of horizontal stresses required to cause 30-degree wide breakouts in rock with a UCS between 900 and 1100 psi, consistent with the breakouts seen intermittently in shallow sediments. In this same stress state, rock strengths greater than 1100 psi, characteristic of most of those sediments, would not break out (see also Slide 44).

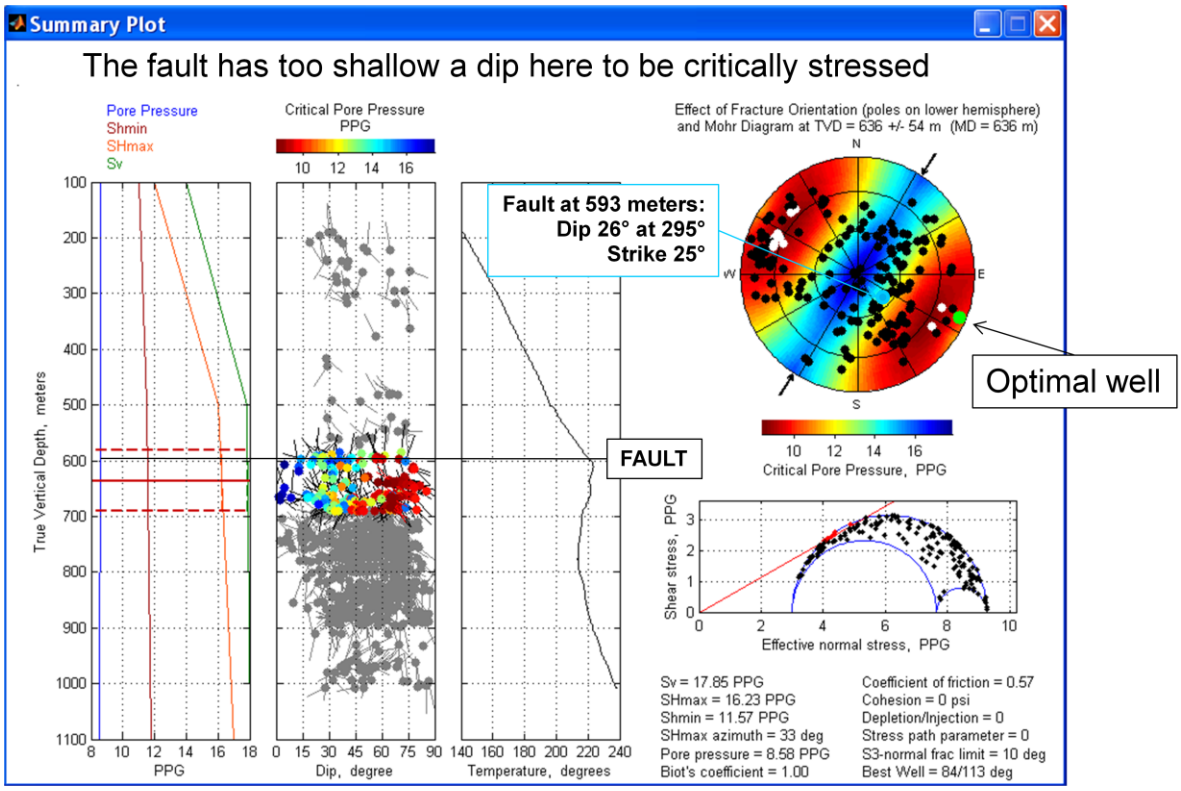

Figure 6: Example of a GMI•MohrFracs™ analysis of fractures in the Alum 25-29 well within the interval of highest temperature. The elevated temperature suggests that this zone is carrying geothermal fluids upwards beneath the detachment fault. Only a few of these fractures is critically stressed; these may provide sufficient permeability to allow such upward flow. The fault detected at 593 meters is not critically stressed, and would not be expected to be hydraulically conductive – it is likely to be a flow barrier.

Implications

- This well is unlikely to be productive, as there is little conductive matrix fracturing except perhaps in shallowest basement, and the fault is too poorly oriented to carry high volumes of geothermal fluids.

- These results are consistent with a model in which fluid flow carries heat upward laterally within uppermost basement, but the flow rate is likely to be quite moderate at this location, in spite of the presence of 3 minor loss zones between 640 and 700 m MD.

- These results are also consistent with results elsewhere in the region where high deliverability only occurs where faults and fractures are critically stressed (which appears not to be the case near this well).

- Intervals of high temperature which indicate lateral convective heat transport do not occur coincident with intervals of resistivity curve separation or high fracture density.

- Places where fractures and/or the fault are more likely to be productive are:

    - Places with a lower magnitude of S_{hmin}

    - Places where the fault dips more steeply

- Given the moderate magnitude of S_{hmin} relative to S_v, it is unlikely that temperature or pressure perturbations from drilling would stimulate seismicity at the Alum site.

Recommendations

- Extended leakoff tests provide an excellent measure of S_{hmin}, and should be run at each casing point.

- Acoustic imaging (e.g., CBIL) is preferred over electrical imaging (e.g., STAR), although as the well builds angle, artifacts associated with tool eccentering (gravity will cause logging tools to lie nearer the low side of the hole) will increase.

- Acoustic (dipole) anisotropy may be useful to reveal intervals of steep, compliant (possibly conductive) fractures.

- Stoneley-wave processing of the existing acoustic data may reveal zones of permeable matrix as well as identify permeable fractures.

- To relate temperature anomalies that indicate fluid exchange / flow zones to features detected on images and logs requires much higher sampling of thermal profiles than is available in Alum 25-29.

- Deliberately deviating wells allows confirmation of the absence of natural vertical fractures at depth, and also allows confirmation that vertical fractures in images within the vertical section were stress induced.